JOURNAL GEOLOGICAL SOCIETY OF INDIA
Vol.83, May 2014, pp.483-492

Lithospheric Structure below Transantarctic Mountain using Receiver Function Analysis of TAMSEIS Data

P. Kumar, Karabi Talukdar and Mrinal K. Sen
National Geophysical Research Institute (CSIR), Uppal Road, Hyderabad - 500 007
Email: prakashk@ngri.res.in

Abstract: The lithospheric structure of Antarctica has been investigated from P- (PRF) and S- receiver functions (SRF) using the seismological data from Trans-Antarctic Mountain Seismic Experiment (TAMSEIS). For the stations deployed on the thick ice sheet, estimation of crustal parameters from PRF may be erroneous as the Moho conversions may interfere with the reverberations within the thick ice sheet. However, the free surface multiples are well observed in PRF. On the other hand, in SRFs, the primary conversions of interest and multiples are separated by the mother S-phase. Therefore, it is advantageous to interpret PRF and SRF jointly for the regions where we have thick low velocity layer at the top such as ice or sediments. The crustal structure and corresponding parameters have already been estimated by various workers, but here we interpret the PRF and SRF jointly to minimize the ambiguity and map the lithospheric architecture below TAM. Our analysis reveals that the average crustal thickness beneath the east Antarctica craton is ~44 km with Vp/Vs ranging between ~1.7 and 1.9. Below Trans-Antarctic Mountain (TAM), the average crustal thickness is ~36 km with higher Vp/Vs of ~1.8-2.0. The rift and the volcanic affected coastal region show erratic depths and Vp/Vs, primarily due to the absence of either primary conversion or multiples in the receiver functions. A small number of stations far from the volcano show that the crust is thinnest (~26 to 34 km thick) in the coastal part. The contribution of this study is the mapping of the lithospheric configuration, not done so far using SRF. The SRF section along a profile spanning E-, W- Antarctica and TAM reveals that the lithospheric thickness in the coast is ~80 km and below TAM it is ~120 km. In the central thick ice cover region, the lithosphere thickens upto ~150 km towards Vostok highlands. The most intriguing feature in our SRF section is that the crust and lithosphere are shallow below TAM compared to the E- Antarctica. Further, we observe a mid-lithospheric low velocity layer confined mostly below TAM, suggesting that the thermal buoyancy could be the prime cause for the upliftment of TAM.

Keywords: Crust, Lithosphere, Receiver functions, Transantarctic Mountain, Antarctica.

INTRODUCTION

The Antarctica is one of the less understood regions on the earth's surface since most of its landmass is covered by thick ice. It is a seismically stable continent, except for Palmer peninsula and the Ross Sea regions where we experience seismic activities. There are several hotspots located in and around the Antarctica, which may have played an important role in shaping the tectonic history of the Gondwana breakup (e.g., Windley, 1995). The notable volcanics are the Mount Bird, Mount Terror, Terra Nova and Mount Erebus located in the coastal region.

Tectonically, Antarctica can be divided into three main regimes, namely, (i) the stable east Antarctic (EA) Precambrian craton, which formed a large portion of the supercontinent – the Gondwana (Dalziel, 1992), (ii) the west Antarctica (WA), which is a chain of islands that is tectonically active and an assemblage of crustal blocks characterized by extension and volcanism during the Cenozoic (Behrendt et al., 1991), and (iii) the Cenozoic Trans-Antarctic Mountains (TAM) system - a conspicuous feature in Antarctica. The TAM also represents the geological boundary between EA and WA, but there are debates about the exact mechanism of TAM's uplift. A number of models have been proposed to explain the uplift of the TAM; these include the delayed phase changes (Smith & Drewry, 1984), simple shear extension (Fitzgerald et al., 1986), various kinds of flexure models (Stern and ten Brink, 1989; Bott and Stern, 1992; ten Brink et al., 1993; ten Brink and Stern, 1992), plastic (Chery et al., 1992) and elastic (van der Beek et al., 1994) necking models, transform-flank uplift (ten Brink et al., 1997), and collapse of a high plateau with a thick crust providing the buoyancy (Studinger et al., 2004). A central question on the origin of the TAM that is still being debated: "was the uplift provided by thermal

buoyancy due to perturbed upper mantle temperatures (e.g., ten Brink et al., 1997), or by a thickened crust (Studinger et al., 2004).

A number of seismological studies have been carried out in the past to decipher the velocity structure below Antarctica. Surface wave dispersion, body wave tomography and attenuation studies demonstrate that the TAM separates the mantle of seismically fast and low attenuation E- Antarctica from that of W- Antarctica (Danesi and Morelli, 2001; Ritzwoller et al., 2001; Sieminski et al., 2003; Morelli and Danesi, 2004; Watson et al., 2006; Lawrence et al., 2006b, Lawrence et al.,2006c). Surface wave and receiver function studies reveal that the TAM contains faster shear wave velocities and thicker crust than the WA Rift System (RS) (Bannister et al., 2000; Bannister et al., 2003; Kanao et al., 2002). P-wave velocity images reveal the presence of a low velocity body till ~400km beneath Mount Erebu volcanic region (Gupta et al., 2009). One of the interesting works using the TAMSEIS experiment data involves joint inversion of P-receiver functions and Rayleigh wave phase velocities by Lawrence et al. (2006a), where they found that the Moho depth varies from ~20 km in the RS to ~40 km beneath the crest of the TAM and in the EA it is ~35, suggesting a flexural mode for the upliftment. Using the joint modeling of S-receiver functions and Rayleigh wave group velocities Hansen et al. (2009) estimated the depth of Moho in E-Antarctica craton to be ~40–45 km, whereas below TAM, it is shallower varying between 35 and 40 km. Estimates of crustal thickness from surface waves and receiver function analysis range from about ~35 to 45 km (Ritzwoller et al., 2001). In the Ross Island region the crustal thickness varies from 18 to 25 km (Behrendt, 1999; Bannister et al., 2003; Lawrence et al., 2006b; Watson et al., 2006). Travel time tomography for TAMSEIS data reveals a low velocity anomaly in the upper mantle near the area of Ross Island extending laterally 50 to 100 km beneath the TAM from the coast (Watson et al., 2006). The presence of a thermal anomaly of this magnitude supports models invoking a thermal buoyancy contribution to flexurally driven TAM uplift, at least in the Ross Island region of the TAM. Recently Finotello et al (2011) analyzed the TAMSEIS data (only 19 stations) using the PRF to demonstrate the crust beneath the TAM. They used both the main conversions and its multiples using H-k stacking method. However, our study consists of 44 seismic stations and the intention here is to map the lithospheric architecture using SRF techniques. We analyzed the SRF along a North-South array in order to map the lithospheric thickness in three different tectonic regimes. The results shed light on the composition and evolution of the Antarctica especially on the genesis of TAM.

DATA AND METHODOLOGY

We use teleseismic earthquake data from Trans-Antarctic Mountain Seismic Experiment (TAMSEIS) consisting of 44 broadband seismic stations (see Figs. 1 and 9). Only those stations where sufficient number of recorded events are available were selected. In the present study, 39 stations extending from Ross Sea to the Vostok Subglacial Highlands, were used. The instruments were deployed from Nov 2000 to Dec 2003 in three arrays (Fig.1) i.e. East-West, North-South and Coastal. The TAMSEIS is the first large-scale broadband seismic experiment in Antarctica in three different arrays. These data have been obtained from the IRIS Data Management Center.

In this study we used the converted wave techniques, namely P-to-s (P receiver function, PRF) (Burdick and Langston, 1977; Langston, 1977; Vinnik, 1977) and S-to-p (S receiver function, SRF) (Farra and Vinnik, 2000). The crustal structure and parameters have already been done by various workers using PRF alone (Lawrence et al., 2006; Finotello et al., 2011), jointly using SRF and surface wave dispersion studies (Hansen et al., 2009) etc. Here we jointly

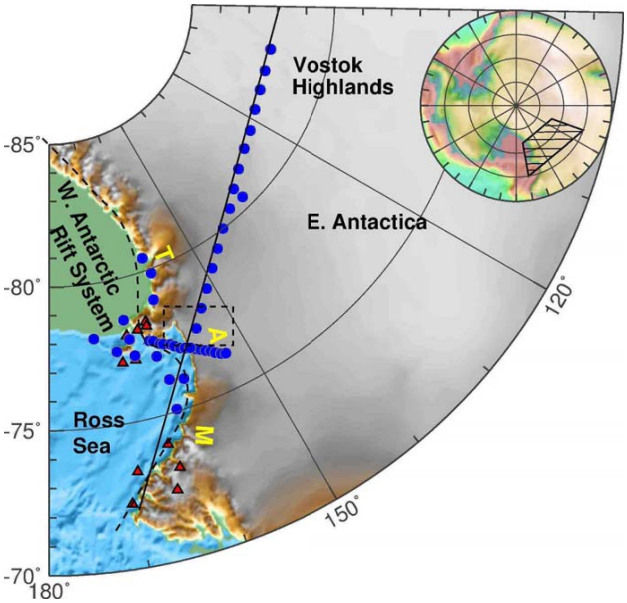

Fig.1. Topographic map of Antarctica with the location of broadband seismic stations (solid blue circles) used in the present study. The shaded region in the key map shows our study region. TAM: Transantartic Mountain. The dashed line is the rift system and dashed box is the approximate location of the TAM. The red triangles are the location of volcano.

interpret the PRF and SRF and present some data examples, but the main focus here is to map the lithosphere below TAM using SRF.

The PRF is used routinely to decipher the crustal and upper mantle seismic parameters from three-component seismic stations utilizing P-to-s conversions from a discontinuity beneath the seismic station, while the SRF looks for S-to-p conversions in the teleseismic range. The latter technique has been proven to be an important tool to detect the uppermost mantle discontinuities such as the Lithosphere-Asthenosphere Boundary (LAB) owing to its advantages over the PRF and thus serves as an important supplement of the former. The advantage of using SRF over PRF is that the former is free from shallow-layer multiples in the time window of arrival of the main converted Sp phases resulting from deeper discontinuities. On the other hand, the converted Ps phases and the shallow layer crustal multiples in PRF fall within the same side of the time window making unique identification of these phases sometime very difficult. This property of SRF is useful in case of thick ice cover region.

We use a large number of seismological data from events with Mb >= 5.6. For PRF analysis we use events within 35°–95° epicentral distance only, while for SRF analysis the events are within 60° – 85°. For computation of PRF, the horizontal seismograms from each event are rotated into radial (R) and transverse (T) components using the back azimuth information. We calculate the radial receiver functions (here we call it PRF) by time-domain deconvolution of the radial components by their respective vertical components in order to remove the source side complications and the propagation effects. On the other hand, for S receiver functions, ZRT- components are further rotated into P-Sv-Sh, the methodology here adopted has been as described by Kumar et al. (2005a, 2005b, 2006) and Kumar & Kawkatsu (2011), where the incidence angle for the rotation is determined by minimizing the amplitudes of P components at S arrival times. The P- and S- receiver functions are moveout corrected at a reference slowness of 6.4 s/deg (Yuan, 1997), using IASP91 earth model (Kennett & Engdahl, 1991) prior to stacking. The time-axis of SRF has been reversed for ease of comparison. Recently, in addition to the P receiver function method, the study of S receiver functions has become a powerful technique to identify the Moho interface, especially when the top layer is a low velocity layer such as the thick ice cover. One such region is Greenland, where Kumar et al (2007) showed the advantage of SRF in combination with PRF to decipher the crustal structure in case of thick ice cover, where the conventional PRF yields ambiguous results.

In order to demonstrate the effect of thick ice sheet as a top layer on RFs, first we generate synthetic receiver functions (Fig.2) (Frederiksen and Bostock, 2000) for two different simple 1-D models. The first model contains no ice at the top layer (Fig.2a) and the second model contains a thick ice layer at the top (Fig.2b). The RFs for no-ice layer at the top has clear conversion from the discontinuity, say the Moho (i.e. Pms and Smp). However, for the model with an ice layer, the Pms has been completely masked by the strong multiples from ice layer in the P-receiver function (see Fig.2). The S-receiver function for the model with an ice layer shows well separated Sip (S-to-p from ice) and Smp. In such a scenario, interpreting both the RFs is useful in deciphering the crustal parameters accurately, where we can take Moho conversion time from SRF and multiples from PRF.

SOME OBSERVED RECEIVER FUNCTIONS EXAMPLES

Here few individual data examples but the stack traces for all the stations are presented. In case of the thick ice

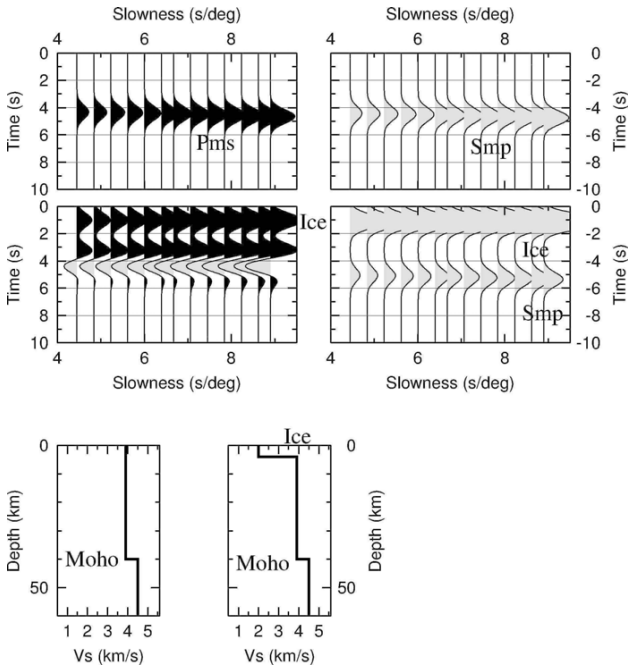

Fig.2. Synthetics P- and S-receiver functions for two different models (bottom panel) without and with an ice layer. In the upper panel, we show PRF in the left and SRF in the right. In the fist case the model contains only one layer Moho, while in second case the model contains Moho and an ice layer at the top. It can be easily seen that the presence of ice sheet has masked the primary conversions from the Moho and make the identification of main phases erroneous (middle right panel).

covered region in the E- Antarctica, the conventional P-to-s conversions yield ambiguous result and thus the estimate of the crustal parameters will be erroneous. Because of this we analyzed both the RFs here and compared the results. Here we present some examples of the observed receiver functions data. Figures 3 to 5 display individual P-receiver function traces along with their corresponding summation traces. The traces for each station are arranged with increasing slowness. The summation boxes of each sub-plot show 2 PRFs and 1 SRF stacked traces. The first and second summation traces are generated after moveout correction for primary phase and for first free-surface multiple respectively. In a hindsight to pick the converted times from Moho and its multiple, the RFs at two different frequencies were analyzed. The sub-plots in Fig.3a, b panel show the traces after low-pass filters with corner frequencies of 1Hz and 0.25Hz respectively. Close examination of the Figures 3 to 5 reveal that the Moho conversion i.e. Pms is clear in 1Hz plot, whereas its multiples are clear in the low-pass 0.25Hz frequency data. The coastal Antarctic region (for example two stations are shown in Figure 3), where we do not record clear Pms all along the slowness range, however, shows that the Smp have earlier times. The stations in Figure 3 are from the coastal regions, which show more scatter in multiple times due to its location in the vicinity of rift and as the multiples sample much more lateral space than the conversions. Figure 4 is data displayed from the east-west array while those in Figures 5 is from the north-south array.

In Fig.3, it can be observed, for the station DIHI more than one multiple times in the stack trace in the time window of 10-20sec, but the primary conversions have nearly constant times. The phenomenon is not apparent in slowness plots as made earlier, however, in azimuthal plot one can observe two arrivals for multiple phases due to their different sampling region as the bounce points for multiples are quite larger. In such scenario the estimation of crustal parameters will be erroneous.

The stack PRF and SRF traces are once again shown in Figures 6 and 7 in order to have station-wise comparison. It is clearly seen that the RF-waveforms for the three different regions look different. The east-west array shows clear Moho conversions which are deepening from west to eastern Antarctica. The icy region stacks in Figure 5 (also Figure 6a) have much larger amplitude just after the Pis (P-to-s conversion from Ice) and the expected Moho arrivals are masked by the negative multiples from ice. The data from north-south array in Fig.6b, clearly show the bifurcation of this phase in the first 1 second from the N036 towards the southern polar side, indicating that the thickness of the ice

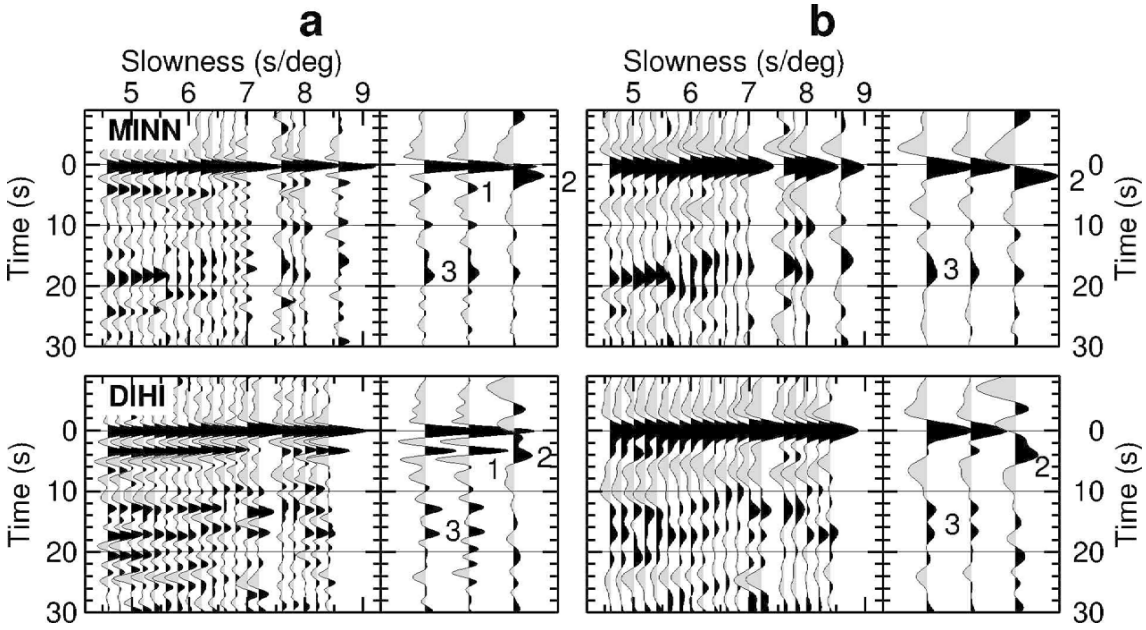

Fig.3. Individual receiver functions with summation traces showing primary conversions and multiple. Also the station stack of the S-receiver function is shown for comparison. These stations are from the coastal Antarctic region. Panel a) is a plot of data with a filter with corner frequency of 1Hz and the panel b) is for the filter with corner frequency of 0.25Hz. The traces have been plotted with narrow overlapping bins in slowness of 0.1s/deg. The higher frequency data shows the crustal and intra-crustal phases clearly whereas in the low frequency plot the multiples are clear visible. Numbers 1 and 2 are the P-to-s (Pms) and S-to-p (Smp) conversion from Crust-mantle boundary respectively. 3 is the multiples (Ppps) between free-surface and the Moho.

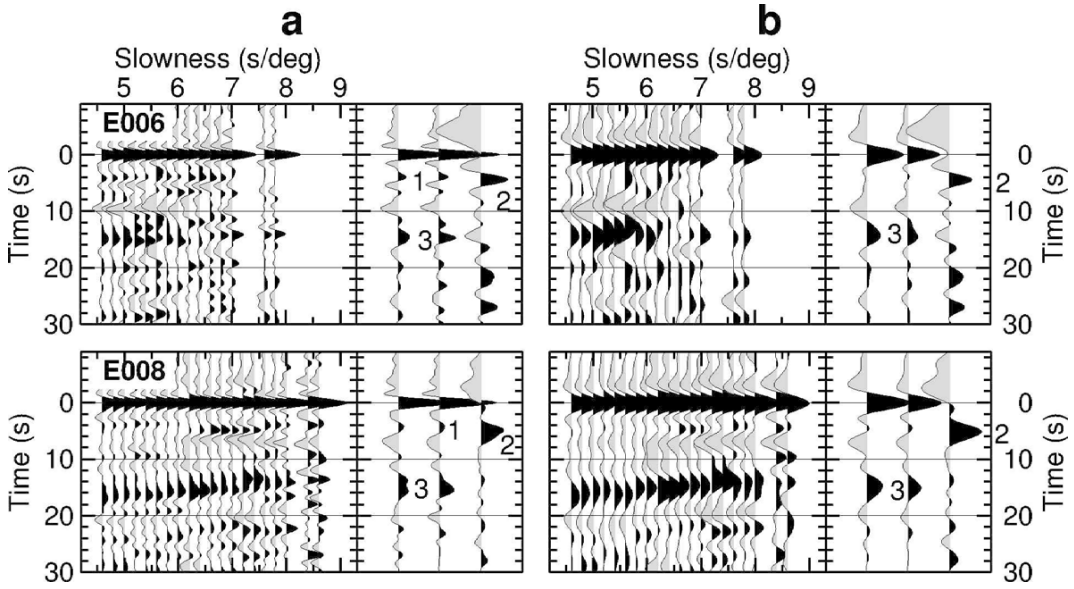

Fig.4. Same as Fig.3, but for the East-West array stations.

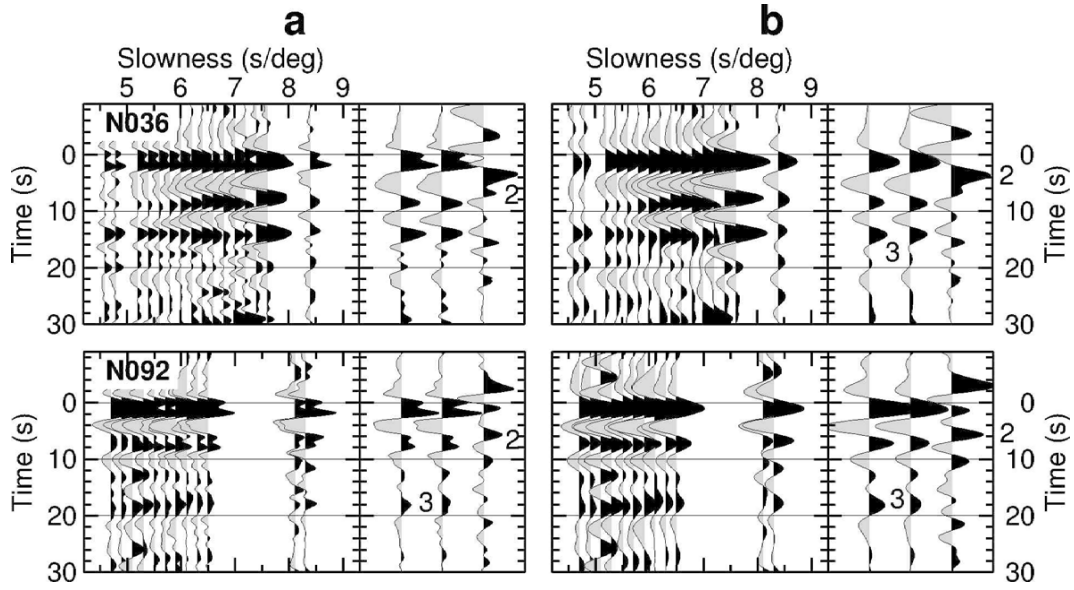

Fig.5. Same as Fig.3, but for the East-West array stations.

sheet is increasing. The waveforms in the data look very similar to those in the synthetics as shown in Figure 2. Similarly, we also plotted the station stacked for S-receiver functions in Figure 7 for all the stations.

LITHOSPHERIC STRUCTURE ALONG NORTH-SOUTH PROFILE

Figure 8 represents the S receiver function wiggle plot along a north-south profile (see Figure 1 and also Figure 9 for the profile location). The section has been made with increasing geographical latitude with stacking over overlapping window. Also the station elevations are plotted at the top (Figure 8a). To plot the wiggle, we took the data from a corridor of width ±100 km on either side of the profile, at a conversion depth of 100 km for S-to-p waves. Here, in order to show the robustness of the identified phases, the data was plotted in three different combinations of overlapping binning windows. In all three sub-plots, it is clear that the labeled phases are robust. The main identified discontinuities are: positive peak is due to ice and observed at ~1s, and the second positive arrival is the Moho converted (Smp) phase which is delayed from ~5s beneath TAM to ~7s beneath East Antarctica. A negative phase (black image)

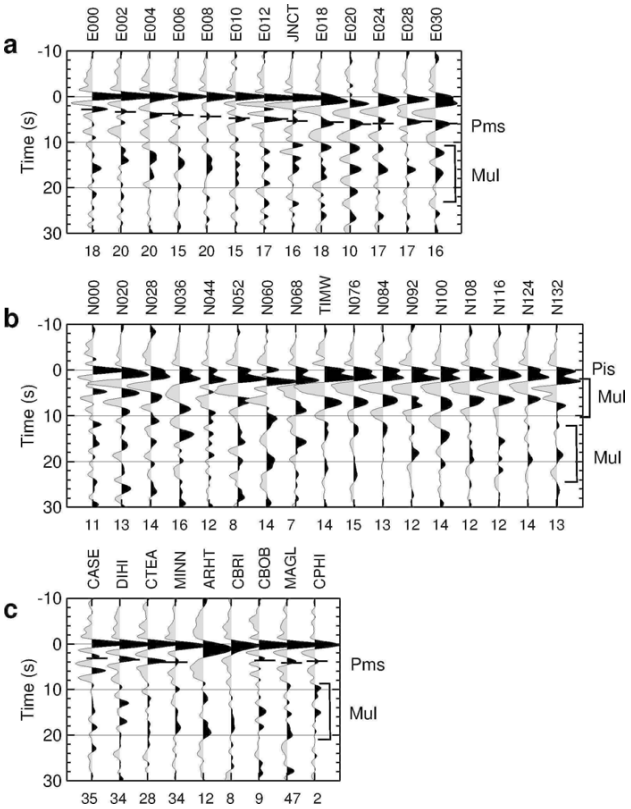

Fig.6. Stacked P-receiver function traces from all the stations used in the present study at frequency of 1Hz. (a) from East-West array, (b) from North-South profile and (c) from coastal stations. The numbers in the bottom abscissa are the number of traces stacked in each single trace. Pms: P-to-s conversion from Moho, Pis: P-to-S conversion from ice layer and Mul: the multiples.

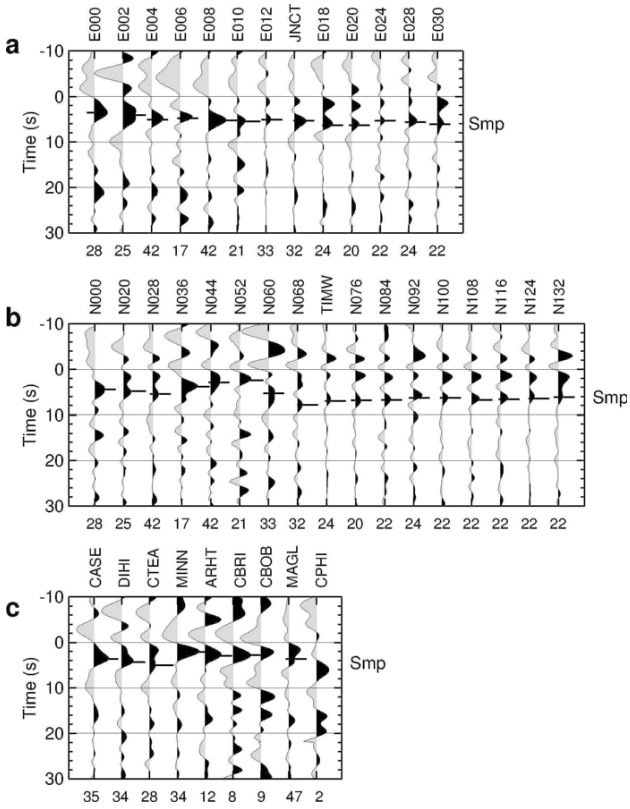

Fig.7. Same as Fig.18 but for S-receiver functions.

is observed at -9 – ~16 s which corresponds to the LAB (lithosphere-asthenosphere boundary) due to the decrease in velocity downward. A low velocity zone (LVZ) in between the Moho and LAB at ~9s and mostly confined just below the TAM is observed. Hence the LAB in the coastal region is at a depth of ~80 km, whereas, for TAM it is observed at ~120 km and for the Precambrian craton East Antarctica, LAB is observed at ~150 km. We observe the thinnest lithosphere in the coastal Antarctica and the thickest towards the EA craton.

DISCUSSION AND CONCLUSIONS

It has been demonstrated numerous times the importance of Antarctica as a key continent for providing constraints to supercontinent reconstruction. Geophysically it is utmost important to know the nature of lithosphere in order to compare it with Gondawana fragments. In order to estimate the average crustal thickness and average crustal Vp/Vs, we picked the Moho conversion times from stacked SRF traces and multiples from PRF summation traces filtered at a frequency 0.25Hz. The Ps converted phases (marked Pms), Sp converted phases (marked Smp) and multiples (Ppms and PpSs+PsPs) are clearly seen in most of the stations. Here we assumed three values of Vp (=6.0, 6.5 and 6.7 km/s) and using the primary conversion time and its corresponding multiple time, depth (Z) and Vp/Vs was estimated (Zandt and Ammon, 1995; Zhu and Kanamori, 2000 etc). The choice of the Vp has less effect on our parameter estimation (Zhu and Kanamori, 2000). The estimated parameters are grouped into three tectonic regimes and plotted in Figure 9. The colours of the stations correspond to the colours of the curves in the right sub-plots. They can be summarized as follows:

- For EA, mostly covered by the north-south profile and partly by the east-west profile, we find that the crust is thick (average thickness of ~44 km) with Vp/Vs of ~1.7-1.9.
- In the WA, the crustal thickness are in between ~26 and 34 km.
- The results are erratic in the coastal region, due to the absence of either some primary or the multiple phase. This is possibly caused by the presence of volcanoes. Note also that the stations are deployed near the rift

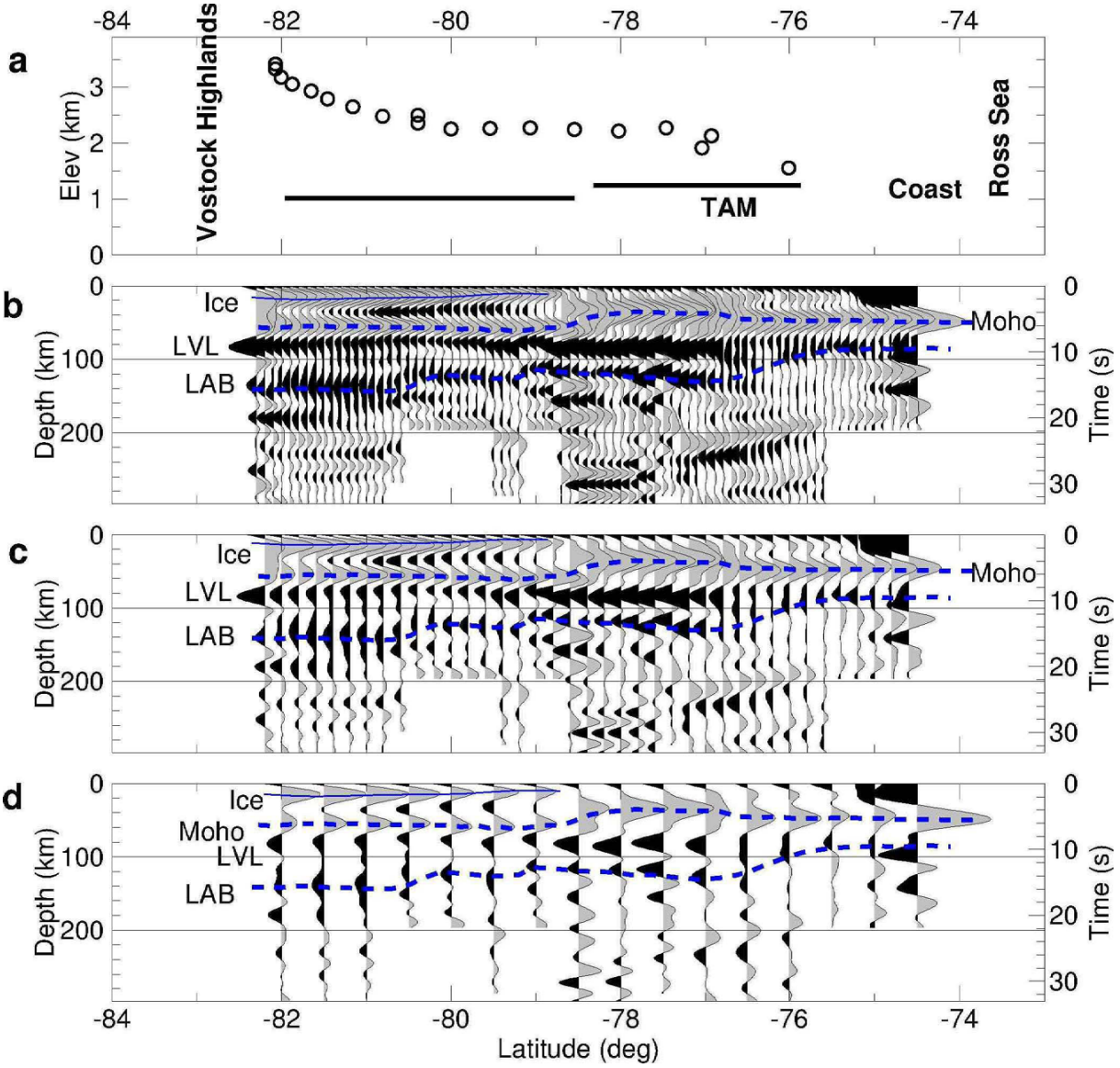

Fig.8. The S-receiver function wiggle plot along a profile shown in Fig.1 (also in Figure 20) using mostly North-South stations. The top subplot (**a**) shows the station elevation and (**b**) to (**d**) are the wiggle plots with three different combination of binning windows. The data of ±1deg on either side of the profile have been projected along the profile. (**b**) is plotted with a step of 0.1deg with a moving window of 0.5 deg, (**c**) is plotted with a bin step of 0.2 deg with moving window of 0.5 deg and (**d**) is generated with a bin step of 0.5 with a moving window of 0.5 deg. In all the wiggle plots the gray is positive and black is negative polarity. In all the plots we observe coherently the Moho, LAB and another feature just below the TAM, a low velocity channel. The time to depth conversions are done using IASP91 model.

systems, which make the region structurally complex.

- Along the NS profile, the Moho depth also increases from the coast inland, changing from 34 km beneath N000 to ~45 km beneath N132.
- The remaining stations CASE, CTEA and DIHI are located on west antarctic rift system. For CASE, the Moho depth is ~34 km, whereas, for CTEA and DIHI it is ~26 and ~30 respectively. The station CPHI is located near the terror rift for which the Moho depth is ~32 km.

The average crustal depths and Vp/Vs are estimated jointly by using PRF and SRF traces. Using these, it is possible to map the lithospheric structure along a profile spanning EA, WA and TAM. The receiver function results suggest that the LAB below Coastal regions is ~80 km, below TAM it is 120 km, and it gets slightly thicker towards EA reaching a value of ~140 km. The crust and LAB below TAM is not thicker than the EA. The SRF profile shows that there is a change in Moho depth just below the

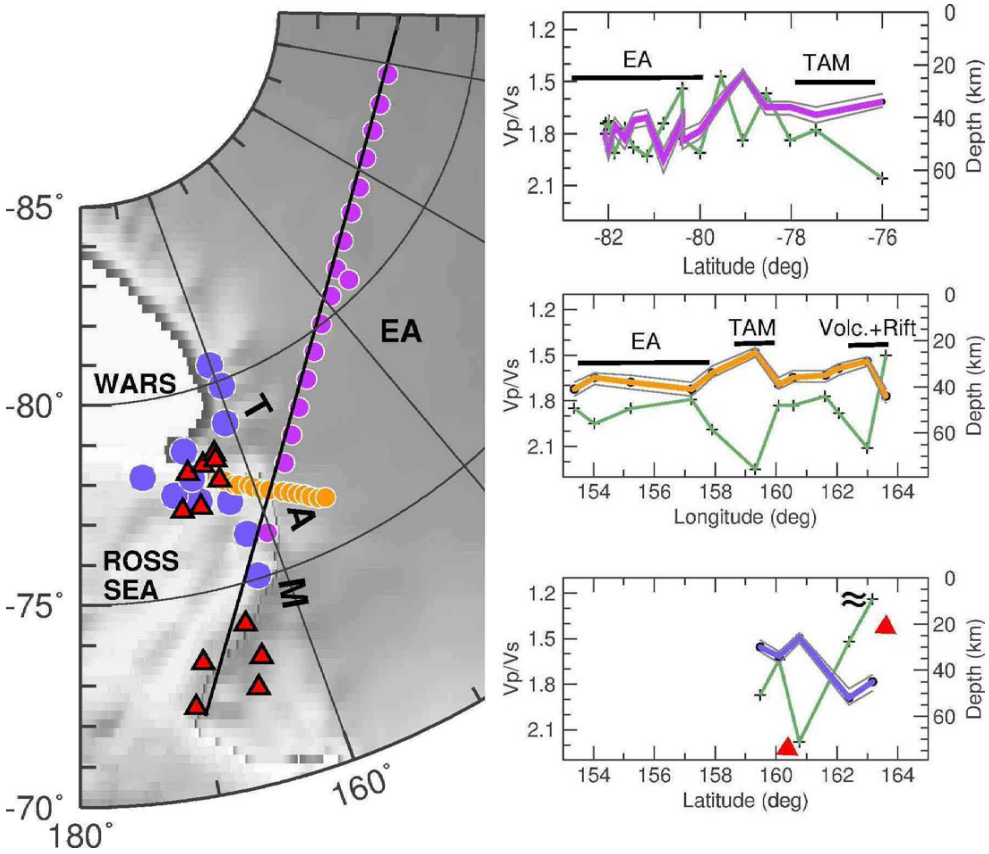

Fig.9. The crustal parameters estimated form PRF and SRF as mentioned in the text. Left map shows the location of seismic stations (Pink, Blue and Yellow solid circles) used in the present study. The red triangles are the volcanos in the coastal region of Antarctica. In the right sub-plots the average crustal depths and Vp/Vs are plotted with the same color as the stations. The green line corresponds to the Vp/Vs plot. The depths are estimated for Vp=6.4 km/s. The color lines for depths are thick due to the fact that the upper and lower depth limit are estimated for Vp=6.0 and 6.7km/s, and these limits will be the error bound in estimated depths.

TAM – the Moho deepens towards the EA. There is an indication of thick sub-Moho low velocity channel within the lithosphere that is mostly confined below the TAM. This channel possibly formed by lateral heat transfer from the rifted WA (Behrendt et al, 1999) causing the upliftment, which resulted in the high elevated mountain range. The presence of a thin lithosphere below TAM is consistent with the result of Fitzgerald et al. (1986), who suggest a lateral and depth dependent asymmetric rifting model for formation of the TAM/WAR region, in which the TAM is underlain by a shallow lithosphere/asthenosphere boundary, created by a detachment zone dipping beneath the mountain belt. Stern and Ten Brink (1989) also suggested that uplift of the TAM was the result of a thermal load under the TAM front, due to lateral heat conduction from the hotter WARS mantle, which aided in the uplift. The uplift may have also been caused by a combination of buoyant thermal load and flexural uplift (Lawrence et al., 2006a). However, thick lithopshere or crust below TAM is not observed in the present study, implying that the lithosphere has been heated by the warm asthenosphere (Smith and Drewry, 1984) that attributes to the uplift of the TAM. In fact Berg et al. (1989) suggest that magma injections into the middle and lower crust of the rift zone increased temperatures that resulted in thermal expansion of the mountain belt. Seismic tomography (Watson et al., 2006) and gravity data (Robinson and Splettstoesser, 1984; Stern and ten Brink, 1989) also suggest similar lithospheric structure beneath EA and the TAMs and corroborate thermally and flexurally driven uplift models for this region of the mountain range. Thus the present findings are more consistent with thermal models, in which the TAMs uplift was driven by buoyancy.

Acknowledgements: Seismological data are from DMC from IRIS. Analysis has been done in SeismicHandler (K. Stammler), and figures were produced using GMT (Wessel and Smith, 1995).

References

BANNISTER, S., SNIEDER, R.K. and PASSIER, M.L. (2000) Shear-wave velocities under the Transantarctic Mountains and Terror Rift from surface wave inversion, Geophys. Res. Lett., v.27, pp.281–284.

BANNISTER, S., YU, J., LEITNER, B. and KENNETT, B.L.N. (2003) Variations in crustal structure across the transition from West to East Antarctica, southern Victoria Land. Geophys. Jour. Int., v.155, pp.870–884.

BEHRENDT, J.C., LEMASURIER, W.E., COOPER, A.K., TESSENSOHN, F., TREHU, A. and DAMASKE, D. (1991) Geophysical studies of the West Antarctic Rift System, Tectonics, v.10, pp.1257–1273.

BEHRENDT, J.C. (1999) Crustal and lithospheric structure of the West Antarctic Rift System from geophysical investigations – a review, Global Planet. Change, v.23, pp.25–44.

BERG, J.H., MOSCATI, R.J. and HERZ, D.L. (1989) A petrologic geotherm from a continental rift in Antarctica. Earth Planet. Sci. Lett., v.93(1), pp.98–108.

BOTT, M.H.P. and STERN, T.A. (1992) Finite element analysis of Transantarctic Mountain uplift and coeval subsidence in the Ross Embayment, Tectonophysics, v.201(3 – 4), pp.341–356.

BURDICK, L.J. and LANGSTON, C.A. (1977) Modeling crustal structure through the use of converted phases in teleseismic body wave forms, Bull. Seism. Soc. Amer., v.67, pp.677-691.

CHERY, J., LUCAZEAU, F., DAIGNIERES, M. and VILOTTE, J.P. (1992) Large uplift of rift flanks: A genetic link with lithospheric rigidity? Earth Planet. Sci. Lett., v.112, pp.195–211.

DANESI, S. and Morelli, A. (2001) Structure of the upper mantle under the Antarctic Plate from surface wave tomography, Geophys. Res. Lett., v.28, pp.4395–4398.

DALZIEL, I.W.D. (1992) Antarctica: A tale of two supercontinents? Annu. Rev. Earth Planet. Sci., v.20, pp.501–526.

FARRA, V. and VINNIK, L. (2000). Upper mantle stratification by P and S receiver functions, Geophys. Jour. Int., v.141, pp.699–712, doi:10.1046/j.1365-246x.2000.00118.x.

FINOTELLO, M., NYBLADE, A. JULIA, J., WIENS, D. and ANANDKRISHNAN, S. (2011) Crustal Vp-Vs tarios and thickness for Ross Island and the Transantarctic Mountain front, Antarctica. Geophys. Jour. Int., v.185, pp.85–92, doi: 10.1111/j.1365-246X.2011.04946.x.

FITZGERALD, P.G., SANDIFORD, M., BARRETT, P.J. and GLEADOW, A.J.W. (1986) Asymmetric extension associated with uplift and subsidence in the Transantarctic Mountains and the Ross Sea Embayment, Earth Planet. Sci. Lett., v.81, pp.67-78.

FREDERIKSEN, A.W. and BOSTOCK, M.G. (2000) Modelling teleseismic waves in dipping anisotropic structures, Geophys. J. Int., 141, 401-412.

GUPTA, S., ZHAO, D. and RAI, S.S. (2009) Seismic imaging of the upper mantle under the Erebus hotspot in Antarctica. Gondwana Res., v.16(1), pp.109-118.

HANSEN, S.E., JULIA, J., NYBLADE, A.A., PYLE, M.L., WIENS, D.A. and Anandakrishnan, S. (2009) Using S-wave receiver functions to estimate crustal structure beneath ice sheets: An application to the Transantarctic Mountains and East Antarctic Craton, Geochem. Geophys. Geosyst., v.10, Q08014, doi:10.1029/2009GC002576.

KANAO, M., SHIBUTANI, T., NEGISHI, H. and TONO, H. (2002) Crustal structure around the Antarctic margin by teleseismic receiver function analyses. *In:* J. A. Gamble, D. N. B. Skinner, and S. Henrys (Eds.), Antarctica at the Close of a Millennium. Royal Soc. New Zealand, Wellington, pp.485–491.

KENNETT, B.L.N. and ENGDAHL, E.R. (1991) Travel times for global earthquake location and phase identification, Geophys. Jour. Int., v.105, pp.429–465, doi:10.1111/j.1365-246X.1991.tb06724.x.

KUMAR, P., ET AL. (2005a). The lithosphere-asthenosphere boundary in the north west Atlantic region, Earth Planet. Sci. Lett., v.236, pp.249–257.

KUMAR, P., YUAN, X., KIND, R. and KOSAREV, G. (2005b) The lithosphere-asthenosphere boundary in the Tien Shan-Karakoram region from S receiver functions: Evidence for continental subduction, Geophys. Res. Lett., v.32, L07305, doi:10.1029/2004GL022291.

KUMAR, P., YUAN, X., KIND, R. and NI, J. (2006) Imaging the colliding Indian and Asian lithospheric plates beneath Tibet, Jour. Geophys. Res., v.111. B06308, doi:10.1029/2005JB003930.

KUMAR, P., KIND, R., PRIESTLEY, K. and DAHL-JENSEN, T. (2007) Crustal structure of Iceland and Greenland from receiver function studies. Jour. Geophys. Res., v.112, B03301, doi:10.1029/2005JB003991.

KUMAR, P. and KAWAKATSU, H. (2011) Imaging the seismic lithosphere-asthenosphere boundary of the oceanic plate, Geochem. Geophys. Geosyst., v.12, doi:10.1029/2010GC003358.

LANGSTON, C.A. (1977) The effect of planar dipping structure on source and receiver responses for constant ray parameter. Bull. Seism. Soc. Amer., v.67, pp.1029–1050.

LAWRENCE, J.F., WIENS, D.A., NYBLADE, A.A., ANANDAKRISHAN, S., SHORE, P.J. and VOIGT, D., (2006a). Crust and upper mantle structure of the Transantarctic Mountains and surrounding regions from receiver functions, surface waves, and gravity: implications for uplift models. Geochem. Geophys. Geosyst., v.7, Q10011. doi:10.1029/2006GC001282.

LAWRENCE, J.F., WIENS, D.A., NYBLADE, A.A., ANANDAKRISHNAN, S., SHORE, P.J. and VOIGT, D. (2006b) Rayleigh wave phase velocity analysis of the Ross Sea, Transantarctic Mountains, and East Antarctica from a temporary seismograph array. Jour. Geophys. Res., v.111, B06302. doi:10.1029/2005JB003812.

LAWRENCE, J.F., WIENS, D.A., NYBLADE, A.A., ANANDAKRISHAN, S., SHORE, P.J. and VOIGT, D. (2006c) Upper mantle thermal variations beneath the Transantarctic Mountains inferred from teleseismic S-wave attenuation. Geophy. Res. Lett., v.33, doi:10.1029/2005GL024516.

MORELLI, A. and DANESI, S. (2004) Seismological imaging of the Antarctic continental lithosphere: a review. Global and Planetary Change, v.42, pp.155–165.

RITZWOLLER, M.H., SHAPIRO, N.M., LEVSHIN, A.L. and LEAHY, G.M.

(2001) Crustal and upper mantle structure beneath Antarctica and surrounding oceans. Jour. Geophys. Res., v.106, pp.30,645 – 30,670.

Robinson, E.S. and Splettstoesser, J.F. (1984) Structure of the Transantarctic Mountains determined from geophysical surveys, in Geology of the Central Transantarctic Mountains, Antarct. Res. Ser., vol. 36, edited by M. D. Turner and J. F. Splettstoesser, pp. 119 – 162, AGU, Washington, D. C.

Sieminski, A., Debyle, E. and Leveque, J.J. (2003) Seismic evidence for deep low-velocity anomalies in the transition zone beneath West Antarctica. Earth Planet. Sci. Lett., v.216, pp.645–661.

Smith, A.G. and Drewry, D.J. (1984) Delayed phase change due to hot asthenosphere causes Transantarctic uplift? Nature, v.309, pp.536–538.

Stern, T.A., and ten Brink, U. S. (1989) Flexural uplift of the Transantarctic Mountains. Jour. Geophys. Res., v.94, pp.10,315 –10,330.

Studinger, M., Bell, R.E., Buck, W.R., Karner, G.D. and Blankenship, D.D. (2004) Sub-ice geology inland of the Transantarctic Mountains in light of new aerogeophysical data. Earth Planet. Sci. Lett., v.220, pp.391–408.

ten Brink, U.S. and Stern, T.A. (1992) Rift flank uplifts and hinterland basins: comparison of the Transantarctic Mountains with the Great Escarpment of southern Africa. Jour. Geophys. Res., v.97, pp.569-585.

ten Brink, U.S., Bannister, S., Beaudoin, B.C. and Stern, T.A. (1993) Geophysical investigations of the tectonic boundary between East and West Antarctica. Science, v.261, pp.45–50.

ten Brink, U.S., Hackney, R.I., Bannister, S., Stern, T.A. and Makovsky, Y. (1997) Uplift of the Transantarctic Mountains and the bedrock beneath the East Antarctic ice sheet. Jour. Geophys. Res., v.102, pp.27,603–27,621.

van der Beek, P., Cloetingh, S. and Andriessen, P. (1994) Mechanisms of extensional basin formation and vertical motions at rift flanks: Constraints from tectonic modeling and fission track thermochronology. Earth Planet. Sci. Lett., v.121, pp.417–433.

Vinnik, L.P. (1977) Detection of waves converted from P to SV in the mantle. Phys. Earth Planet. Int., v.15, pp.39-45.

Watson, T., Nyblade, A., Wiens, D.A., Anandakrishnan, S., Benoit, M., Shore, P.J., Voigt, D. and VanDecar, J. (2006) P and S velocity structure of the upper mantle beneath the Transantarctic Mountains, East Antarctic craton, and Ross Sea from travel time tomography, Geochem. Geophys. Geosyst., 7, Q07005, doi:10.1029/2005GC001238.

Wessel, P. and Smith, W.H.F. (1995) New version of the Generic Mapping Tools released, Eos Trans. AGU, 76, 33, doi:10.1029/95EO00198.

Windley, B.F. (1995) The Evolving Continents, 3rd Ed. John Wiley and Sons, UK. 526p.

Yuan, X., Ni, J., Kind, R., Mechie, J. and Sandvol, E. (1997) Lithospheric and upper mantle structure of southern Tibet from a seismological passive source experiment. Jour. Geophys. Res., v.102, pp.27,491–27,500, doi:10.1029/97JB02379.

Zandt, G. and Ammon, C.J. (1995) Continental crust composition constrained by measurements of crustal Poisson's ratio, Nature, v.374, pp.152–154.

Zhu, L. and Kanamori, H. (2000) Moho depth variation in southern California from teleseismic receiver functions. Jour. Geophys. Res., v.105, pp.2969–2980.

(Received: 29 April 2013; Revised form accepted:20 May 2013)